Room-temperature spin-lifetime anisotropy exceeding 60 in bilayer graphene spin valves proximity coupled to WSe_2

To cite this article: Timo Bisswanger *et al* 2026 *2D Mater*. **13** 015025

2D Materials

PAPER

OPEN ACCESS

RECEIVED
6 June 2025

REVISED
11 December 2025

ACCEPTED FOR PUBLICATION
16 December 2025

PUBLISHED
19 January 2026

Room-temperature spin-lifetime anisotropy exceeding 60 in bilayer graphene spin valves proximity coupled to WSe_2

Timo Bisswanger[1,3], **Anne Schmidt**[1,3], **Frank Volmer**[1], **Christoph Stampfer**[1,2] **and Bernd Beschoten**[1,*]

[1] 2nd Institute of Physics and JARA-FIT, RWTH Aachen University, 52074 Aachen, Germany
[2] Peter Grünberg Institute (PGI-9), Forschungszentrum Jülich, 52425 Jülich, Germany
[3] T Bisswanger and A Schmidt contributed equally to this work.
[*] Author to whom any correspondence should be addressed.

E-mail: bernd.beschoten@physik.rwth-aachen.de

Keywords: bilayer graphene, spin transport, spin orbit proximity coupling, spin lifetime anisotropy

Supplementary material for this article is available online

Abstract

A spin lifetime anisotropy between in-plane and out-of-plane spins in bilayer graphene (BLG) can be achieved by spin–orbit proximity coupling of graphene to transition metal dichalcogenides. This coupling reduces the in-plane spin lifetime due to proximity-induced spin scattering, while the out-of-plane spin lifetime remains largely unaffected. We show that at room temperature spin lifetime anisotropy exceeds 60 in a BLG lateral spin valve proximity coupled to WSe_2. The out-of-plane spin lifetime of about 250 ps closely matches that of a BLG reference region not in contact with WSe_2. In contrast, the estimated in-plane spin lifetime of less than 4 ps leads to a complete suppression of the in-plane spin signal measured at the ferromagnetic Co/MgO spin detector. The proximity coupling of WSe_2 to BLG is particularly promising, as it does not compromise the charge carrier mobility within the graphene channel.

1. Introduction

A promising method to manipulate the spin transport in graphene-based spin-valve devices is to couple the graphene transport channel to a material with high spin–orbit coupling [1–3]. Such materials include transition metal dichalcogenides (TMDs) like WSe_2, WS_2, $MoSe_2$, MoS_2 or their alloys [4–6], but also materials like topological insulators or two-dimensional magnetic insulators, where the latter includes composites such as $Cr_2Ge_2Te_2$ or $MnPSe_3$ that can induce ferro- or antiferromagnetic proximity exchange coupling in graphene [7–9]. Due to their strong SOC, TMDs that are proximity-coupled to graphene imprint an effective out-of-plane spin orbit field on the graphene layer, which enhances spin scattering for spins oriented in the graphene plane while leaving out-of-plane spins largely unaffected [1, 4, 5, 7, 10, 11]. This yields a pronounced spin lifetime anisotropy, defined as $\xi = \tau_\perp/\tau_\parallel$, between the out-of-plane ($\tau_\perp$) and in-plane ($\tau_\parallel$) spin relaxation times [12].

In lateral spin-valve experiments on TMD/single-layer graphene (SLG) heterostructures utilizing MoS_2, $MoSe_2$, WS_2, and $PdSe_2$ spin-lifetime anisotropies of about $\xi \approx 10$ have been reported so far [13–16], whereas the theoretical expectation is at least one order of magnitude higher [10]. Furthermore, the anisotropy in these studies was not sufficiently high enough to completely suppress the in-plane spin signal from reaching the detector electrode [13–16]. Even though WSe_2 has already been used in lateral spin valves, no anisotropy was determined or quantified that way [17, 18], but in weak anti-localization measurements on WSe_2/SLG/hexagonal boron nitride (hBN)-heterostructures at temperatures below 2 K a lower bound of $\xi = 20$ has been found [19].

Furthermore, using bilayer graphene (BLG) instead of single layer graphene offers additional opportunities for graphene-based spintronic devices that are proximity coupled to TMDs. Electrical transport measurements in BLG devices that are in contact with TMDs on either one or both sides reveal

that the proximity-induced SOC is layer-selective, primarily impacting the graphene layer in direct contact with the TMD [20–22]. Combined with the fact that the band structure of BLG can be tuned with out-of-plane electric fields to either open a bandgap [23] or to confine all charge carriers to only one of the two layers [24], enables device concepts such as spin–orbit valves or spin transistors [4, 24]. In this respect, a BLG spin-valve that was fully supported by a large WS_2 flake has already shown a spin-lifetime anisotropy of about $\xi = 40 \ldots 70$ albeit at low temperatures of 4 K [25]. However, much higher values up to $\xi = 10\,000$ were theoretically predicted in BLG proximity-coupled to WSe_2 [4]. At the same time, WSe_2 is a substrate that leaves the charge carrier mobility largely unaffected in its graphene-based heterostructures [26, 27]. Therefore, WSe_2 is expected to be particularly suitable for introducing high spin lifetime anisotropy into graphene-based spin valves through proximity coupling, while retaining its charge transport properties.

Here we report a room temperature (RT) spin-lifetime anisotropy with a lower bound of 60 obtained in a lateral spin-valve device consisting of BLG coupled to WSe_2. The high anisotropy leads to a complete suppression of the in-plane spin signal measured at the ferromagnetic detector electrode in both in-plane Hanle and spin-valve measurements. Instead, the spin signal could be recovered in oblique Hanle measurements and x-Hanle measurements involving the out-of-plane spin component [28–31]. Because of the full suppression of the in-plane component, the respective lifetime was estimated by numerical simulations of the angle-dependent, anisotropic spin precession data to be less than 4 ps.

2. Results and discussion

The device discussed here is built from exfoliated BLG on a Si^{++}/SiO_2 (285 nm) substrate, where one part of the BLG transport channel is proximity coupled to a multilayer WSe_2 flake with a thickness between 4 and 7 nm determined by optical contrast measurements in the heterostructure region (see figures 1(a) and (b)). The WSe_2 flake was placed across the BLG with a dry transfer technique using a PDMS-droplet [32] and is located in sample region C in figure 1(b), further referred to as the 'WSe_2 region'. Two uncovered regions labeled A and B in figure 1(b) serve as reference regions to characterize spin transport. The spin-sensitive electrodes were fabricated from 3 nm magnesium oxide (MgO), serving as spin injection/detection barriers, and 35 nm cobalt (Co) [33, 34], both deposited under ultra-high vacuum conditions [35]. The contact-resistance-area products of the fabricated electrodes were in the range of 2.4–7.2 $k\Omega\mu m^2$. The width of the BLG flake in the investigated regions is in the range of 1.1–1.5 μm and the contacts have a width of 450–800 nm in the x-direction (see figure 1(d) for coordinate system). For such a contact geometry only a single magnetic domain is formed with its easy-axis along the y-direction [36]. A magnetic field in either the x-direction (in-plane perpendicular to the contacts) or in the z-direction (out-of-plane) slowly rotates the magnetization from the easy-axis with increasing field strength [37], which we accounted for in our data analysis by a Stoner–Wohlfarth model [14, 38, 39]. All measurements were performed at RT. For the non-local spin transport measurements a low-frequency lock-in technique was used with a frequency of $f = 21$ Hz and an AC current of $I_{AC} = 10\,\mu$A added on a DC current of $I_{DC} = 25\,\mu$A [40].

The WSe_2 region exhibits a charge carrier mobility of 5800 $cm^2\,(Vs)^{-1}$, as determined from gate-dependent conductance measurements [32]. The mobility is comparable to mobility values of 5200 $cm^2\,(Vs)^{-1}$ and 6800 $cm^2\,(Vs)^{-1}$ for the reference regions A and B, respectively. We therefore conclude that the presence of WSe_2 in these heterostructures on SiO_2 the WSe_2 does not adversely affect the charge carrier mobility in BLG. This observation is consistent with previous studies on high-quality, fully encapsulated graphene devices, which demonstrated that WSe_2 substrates allows for charge carrier mobilities comparable to, or even exceeding, those achieved with hBN encapsulation [27, 41].

2.1. Spin transport in the reference regions

We first study the spin transport properties of the reference regions by performing spin-valve and Hanle measurements at RT at zero gate voltage near the charge neutrality point in a non-local configuration (figure 1(a)). For the spin-valve measurements, the magnetic field is changed in its magnitude along the y-direction (see figure 1(c)), i.e. at angle $\beta = 0°$ between the y and z-direction. Figure 2(a) shows the measurement of region A. The spin-valve measurement (black curve) shows typical switching with a non-local resistance ΔR_{nl} of about 2.5 Ω (3.6 Ω for region B). From the spin precession measurements in Hanle configuration with a magnetic field perpendicular (i.e. $\beta = 90°$) to the sample plane (red curve in figure 2(a)), the spin lifetime τ_s and spin diffusion length λ_s were determined with the steady-state solution of the Bloch–Torrey equation [42, 43]. To better distinguish the different measurement configurations, we will further refer to this as z-Hanle. The corresponding spin lifetime is 360 ps (280 ps for region B) with a spin diffusion length of $\lambda_s = 2.8\,\mu$m (1.7 μm for region B).

In the z-Hanle measurement, the spin precession takes place entirely in the sample plane (x–y-plane). Therefore, to measure the spin-lifetime anisotropy,

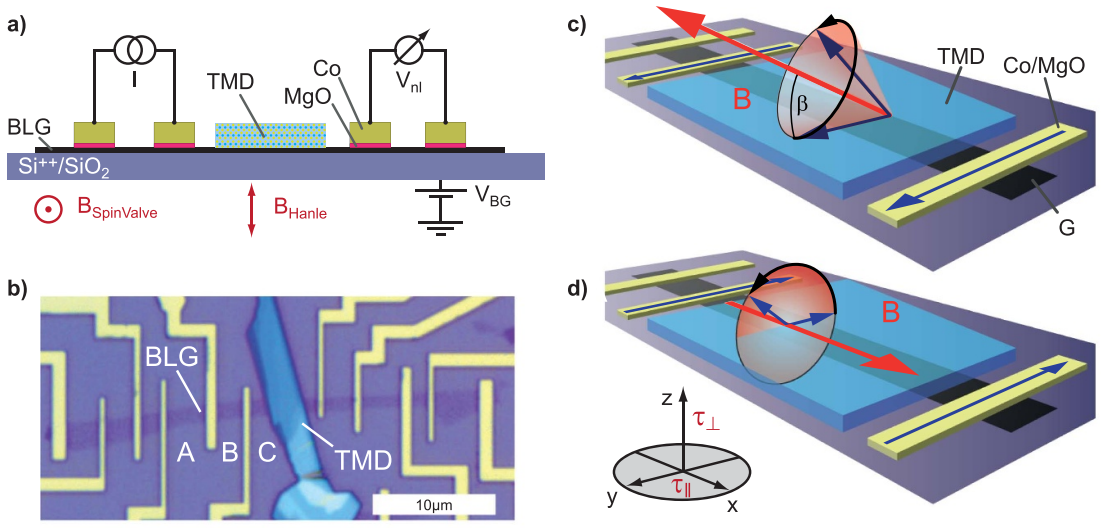

Figure 1. (a) Schematic cross-section of the device illustrating the stacking order and the wiring in case of a non-local spin transport measurement. (b) Optical image of the device with the reference regions A and B and the WSe_2 (TMD) proximity coupled region C. (c) In case of the oblique Hanle measurement, the external magnetic field is oriented at an angle β between the easy-axis of the ferromagnetic electrodes (blue arrows) ($\beta = 0°$) and the out-of-plane field direction of a standard Hanle spin precession measurements ($\beta = 90°$). (d) In the x-Hanle configuration the external magnetic field points in the x-direction, which is defined as the direction perpendicular to the ferromagnetic contacts and within the plane of the graphene channel.

the spins must acquire an out-of-plane component during their precession. This can be achieved with two different measurement schemes: (1) in oblique Hanle measurements (figure 1(c)) the magnetic field is applied at an angle β between $\beta = 0°$ and 90°, so that an angle-dependent out-of-plane component is obtained due to the tilted precession of the spins. (2) For x-Hanle, the magnetic field is applied in the x-direction, i.e. in-plane but perpendicular to the contacts, which is illustrated in figure 1(d). During precession, the spins gain an out-of-plane component as they now precess in the y–z plane.

For reference region A, we discuss first the oblique Hanle measurements. A selection of the corresponding curves recorded at different angles β is given in figure 2(b). The curves appear as a combination of spin-valve (0°) and z-Hanle measurements (90°). The spin-lifetime anisotropy was determined following the evaluation proposed by [29, 39]: at higher magnetic fields (150 mT), the spins are assumed to be fully dephased, leading to a saturation value that depends on angle and anisotropy. The dependence on anisotropy as derived in [28, 29] is as follows:

$$\frac{R_{\mathrm{nl}\beta}}{R_{\mathrm{nl}0}} = \chi^{\frac{1}{2}} \exp\left[\frac{-L}{\lambda_{\parallel}}\left(\chi^{-\frac{1}{2}} - 1\right)\right] \cos^2\beta, \quad (1)$$

where

$$\chi = \left(\cos^2\beta + \xi^{-1}\sin^2\beta\right)^{-1}, \quad (2)$$

where L is the channel length, $\lambda_{\parallel} = \sqrt{\tau_{\parallel} D_s}$ represents the in-plane spin diffusion length, $R_{\mathrm{nl}\beta}$ is the non-local resistance in the saturation regime measured at angle β, and $R_{\mathrm{nl}0}$ is the value at $B = 0$. The spin lifetime anisotropy ξ becomes the only fit parameter when $\tau_{\parallel}$ and D_s are determined independently from the z-Hanle measurement.

The saturation resistance of the reference region $R_{\mathrm{nl}\beta}$ is normalized with $R_{\mathrm{nl}0}$ and plotted in figure 2(d) against $\cos^2(\beta)$. In an isotropic case ($\tau_{\perp} = \tau_{\parallel}$), a linear relationship versus $\cos^2\beta$ is expected as indicated by the straight line in figure 2(d) [13]. For anisotropies $\xi > 1$ (< 1), the curve would be above (below) the $\xi = 1$ curve (black line). The fit to our data (red line) gives an anisotropy of $\xi = 1.19$. According to [28] a value slightly above 1 can be explained by small out-of-plane spin–orbit fields that are caused by ripples or flexural distortions. However, in our sample we also observe that the oblique Hanle curves do not completely saturate even at higher magnetic fields as can be seen in the non-vanishing slope above 150 mT in all curves with $\beta \neq 0$ in figure 2(b). This slope can be explained by a Hall signal, that is caused by a spatially inhomogeneous injection of charge carriers through pinholes in the MgO barrier [44]. Since this Hall signal depends on the magnetic field direction (see [44]), it also varies with β and therefore influences the previously described method for evaluating the spin lifetime anisotropy.

To investigate this possible source of error with regard to the extracted spin lifetime anisotropy further, we performed x-Hanle measurements (figure 2(c)), in which the in-plane direction of the magnetic field does not result in any Hall voltages.

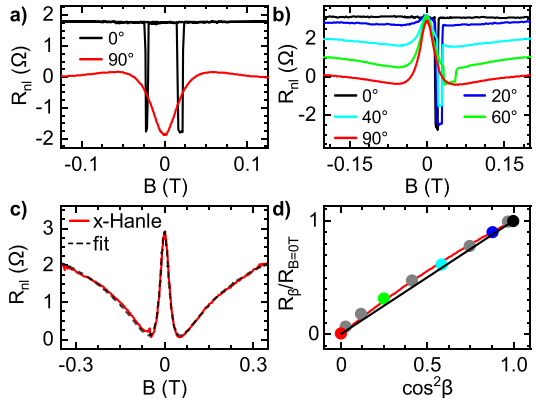

Figure 2. Results for BLG reference regions. (a) z-Hanle (90°) and spin-valve measurements (0°) of reference region B. (b) Oblique Hanle in reference region A at selected angles. (c) x-Hanle measurement with fit (black dotted curve), and (d) the evaluation of the anisotropy from the oblique Hanle measurements for reference region A. The colored dots relate to the curves shown in (b), the black straight line corresponds to $\xi = 1$, and the red line is the fit to the data.

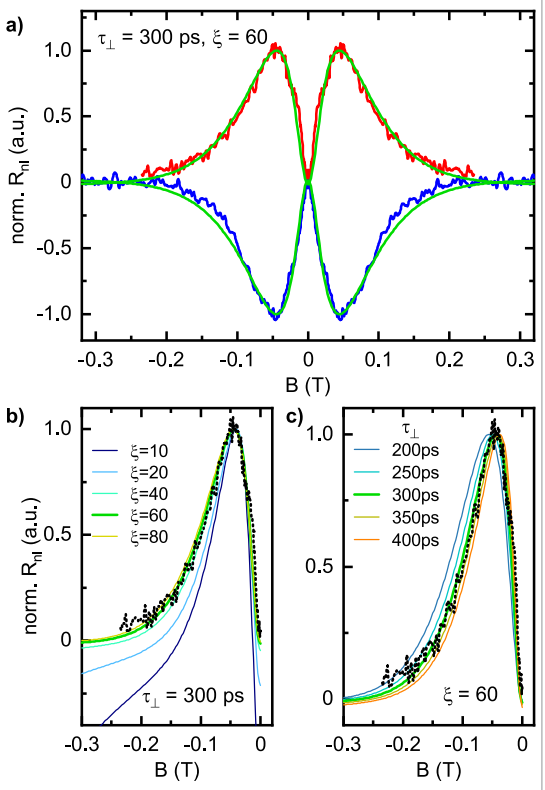

Figure 3. x-Hanle measurement and its numerical simulations in the WSe_2 region. (a) x-Hanle measurement and best simulation result (green lines) with $\tau_\perp = 300$ ps and $\xi = 60$. (b) Variation of the spin-lifetime anisotropy ξ for a constant $\tau_\perp = 300$ ps. (c) Variation of $\tau_\perp$ for a constant $\xi = 60$. The spin diffusion coefficient is set to 0.025 $m^2\,s^{-1}$ for the simulations.

In the isotropic case, the shape of the curve is expected to be identical to the z-Hanle curve, since the projection of the precessing spin ensemble on the y-direction (direction of the magnetization of the contacts) is identical regardless if the spins precess in the z–y- or x–y-plane. However, due to the shape anisotropy of the contacts, the magnetization of the contacts rotates significantly more when applying the magnetic field along the x-direction than along the z-direction [37]. The more the magnetization rotates towards the magnetic field direction, the larger the overall contribution of the injected spins (which are injected parallel to the magnetization) that is parallel to the external field. This non-precessing contribution of the injected spins results in an additional background signal, that increases the more the magnetization is rotated away from the y-direction. This background is seen in a figure 2(c) as a steadily growing signal away from $B = 0$ in both directions, while R_{nl} above $|B| > 150$ mT in the z-Hanle configuration approaches $R_{nl} = 0$ (see figure 2(a)).

We implemented a Stoner–Wohlfarth model [14, 38, 39, 45] in the steady-state solution of the Bloch–Torrey equation [43] to account for the rotation of the magnetization of the contacts in the x-Hanle measurement scheme. With the adapted fit (see dashed black line in figure 2(c), we find a spin-lifetime of 350 ps in reference region A, which is within the fit error identical to the lifetime extracted from the z-Hanle measurement (360 ps). This implies an anisotropy factor of 1, as expected from graphene without any proximity coupling [39], in contrast to the value of 1.19 extracted from the oblique Hanle method. This indicates that charge-induced Hall signals must be considered if precise anisotropy values are to be extracted from oblique Hanle measurements.

2.2. WSe_2 proximity-coupled region

In contrast to the uncovered BLG regions A and B, we could not detect any spin signal in the WSe_2 region in either spin-valve configuration ($\beta = 0°$) or z-Hanle configuration ($\beta = 90°$) (see black and gray lines in figure 4(a). Spins injected in-plane obviously do not reach the detector as long as their orientation remains in-plane due to an extremely short in-plane spin lifetime. Since higher out-of-plane spin lifetimes are expected within the WSe_2 proximity-coupled region, we next performed oblique Hanle and x-Hanle measurements in the electron conduction regime at a charge carrier density of $n = 2 \times 10^{12}\,cm^{-2}$.

Figure 3(a) shows the x-Hanle measurements for both parallel and antiparallel orientation of the injection and detection electrode's magnetization. To limit the impact of charge-induced background signals, the spin signal for each orientation was symmetrized and normalized according to $R_{symm} := (|R_{nl}(-B)| + |R_{nl}(B)|)/2 - R_{nl}(B = 0)$. As expected from the z-Hanle measurements, the spin signal is zero at $B = 0$ T. Instead, for increasing magnetic field strength the spin signal first increases due to an increased out-of-plane contribution, before it decreases again due to magnetic field-induced dephasing of the spin

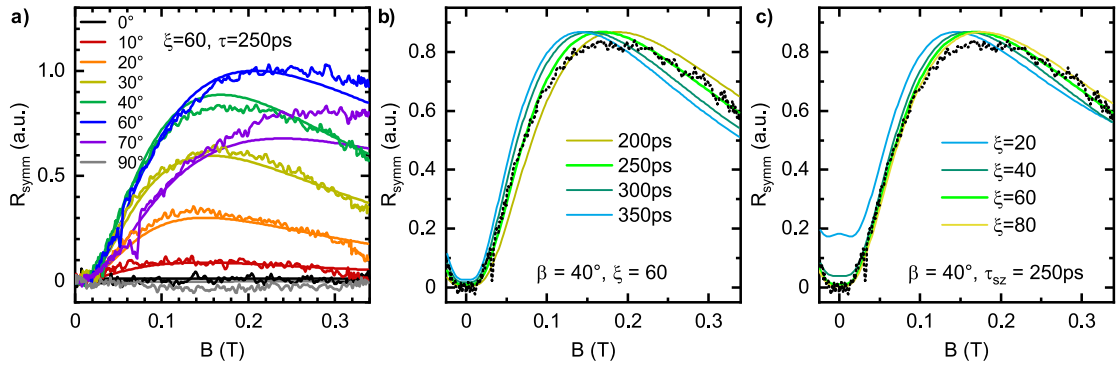

Figure 4. Symmetrized and normalized oblique Hanle measurements of the WSe_2-region and simulation curves. (a) Measurement set at different angles β with corresponding simulations using the best match parameters from (b) and (c), i.e. $\tau_\perp = 250$ ps and $\xi = 60$. (b) Measurement at $\beta = 40°$ and simulated curves for which the spin-lifetime anisotropy $\xi = 60$ was kept constant while varying the out-of-plane spin lifetime $\tau_\perp$. (c) Similarly to (b) $\tau_\perp = 250$ ps is kept constant while varying ξ. The spin diffusion coefficient is set to 0.025 $m^2\,s^{-1}$ for the simulations.

ensemble (see also [14]). Unfortunately, fitting these curves with the anisotropic solution of the Bloch–Torrey equation proposed in [31] is not possible, as this fitting procedure requires a pre-determined in-plane spin lifetime and spin diffusion coefficient extracted from z-Hanle measurements, which is not possible in our device as the in-plane spin transport is fully suppressed.

However, a numerical simulation of the anisotropic spin-precession data is possible, using a three-dimensional approach of the Bloch–Torrey equation in COMSOL Multiphysics® software, adapted from the model presented in [45]. Assuming that charge and spin diffusion coefficients are identical for each region, we use the previously determined spin diffusion coefficient of the reference region in our simulations due to similar mobilities between the regions. The best simulation of the z-Hanle measurement was achieved by assuming an out-of-plane spin lifetime of $\tau_\perp = 300$ ps with a spin lifetime anisotropy of $\xi = 60$ (green curve in figure 3(a)). For comparison, figure 3(b) shows simulations with a constant out-of-plane spin lifetime of 300 ps but with different spin lifetime anisotropies $\xi = 10 \ldots 80$. We find that the simulation approximates the shape of the curve well for values of $\xi \geqslant 60$ without being able to give an upper limit. Similarly, figure 3(c) depicts the simulation results for the estimated anisotropy of $\xi = 60$ for varying out-of-plane spin lifetimes.

In a next step, we conducted oblique Hanle measurements in the WSe_2 region as shown in figure 4(a). The respective measurements in spin-valve and z-Hanle configuration, corresponding to $\beta = 0°$ and 90°, show no features above the noise level, as mentioned earlier. Instead, a spin signal appears for intermediate angles. Typical evaluation methods for this kind of data set as proposed in [28, 29, 31, 46] are again not applicable in our case, as they require a residual spin signal for $\beta = 0°$ and 90° to obtain reference values. We therefore again apply numerical simulations to find a best set for $\tau_\perp$ and ξ that can describe the entire set of curves.

Starting with the best match values from the x-Hanle simulations, we examine the simulation results at an angle of $\beta = 40°$ for different out-of-plane spin lifetimes for a fixed value of the anisotropy of $\xi = 60$ in figure 4(b). Only a lifetime of $\tau_\perp = 250$ ps (green curve) follows the experimental data (black points) reasonably well over the whole magnetic field range. Shorter lifetimes underestimate the data for smaller fields and overestimate it for higher fields. The exact opposite (e.g. overestimation for small fields and underestimation for higher fields) is seen in case of higher spin lifetimes.

Figure 4(c) shows the corresponding simulation results for different spin lifetime anisotropies with a fixed spin lifetime of $\tau_\perp = 250$ ps. The variation of ξ has its most pronounced effect around $B = 0$ T. For smaller values of ξ, a residual in-plane spin signal in the form of a small Hanle peak appears at $B = 0$ T, as measured in previous studies [13, 25, 39]. As was the case with the x-Hanle simulations, we find that the simulation approximates the shape of the curve well for values of $\xi \geqslant 60$ without being able to give an upper limit. The best-match values obtained this way ($\xi = 60$ and $\tau_\perp = 250$ ps), also quite well simulate the oblique data set for every other angle β (see solid lines in figure 4(a). Smaller deviations between experimental data and simulations can be explained by signals caused by the Hall effect [40, 44], which was not considered in our model.

2.3. Underestimation of the spin lifetime anisotropy

Although the extracted spin lifetime anisotropy of $\xi \geqslant 60$ is one of the highest values reported in literature so far, it remains well below the theoretical prediction of up to $\xi = 10\,000$ in case of BLG proximity-coupled to WSe_2 [4]. The most likely explanation for this is that we have neglected the impact of contacts

and substrates on the measured spin lifetimes. It has been demonstrated that using the steady-state solution of the Bloch–Torrey equation [42, 43] without considering contact- or substrate-induced spin relaxation processes leads to an underestimation of the extracted spin lifetime [34, 46–54].

The measured total spin relaxation rate (i.e. the inverse of the measured spin lifetime) is the sum of contributions from spin relaxation rates due to the contacts, the SiO_2 substrate and the proximity-induced out-of-plane spin orbit field caused by the TMD. Assuming that only the latter exhibits an anisotropy between out-of-plane and in-plane spin lifetimes, whereas the spin relaxation rates due to the SiO_2 substrate and the MgO/Co contacts are the same for both spin orientations, we can make the following reasoning: In case of the in-plane spin lifetime, the complete suppression of the in-plane spin component implies that the proximity-induced out-of-plane spin orbit field completely dominates over other relaxation channels. The opposite is true for the out-of-plane spin lifetime, as it is very similar to the spin lifetime in the reference region, implying that substrate- and contact-induced relaxation rates dominate here.

At the same time, it was shown that spin lifetimes of up to 12 ns can be reached in graphene-based spin valve devices [55]. This implies that the determined out-of-plane spin lifetime of 250–300 ps could, in principle, be enhanced by at least a factor of 40, if substrate- and contact-induced relaxation processes could be diminished. Under such conditions, the corresponding spin lifetime anisotropy could potentially increase to $\xi = 60 \times 40 = 2400$, bringing it much closer to the theoretically expected value of $\xi = 10\,000$.

Furthermore, we note that the twist angle between the TMD and BLG might also have an impact on the anisotropy. Prior studies have demonstrated that the strength of the SO proximity effect depends on the twist angle [9, 56–62]. In our sample, we estimate the twist angle between the flakes to be approximately 18°, based on microscope images and the assumption that the flakes have ripped along the same crystallographic axes during exfoliation. This estimated angle falls in the regime of strong Valley–Zeeman coupling [56, 59] which favors large spin lifetime anisotropies. However, further studies are required to determine the dependence of twist angle on spin lifetime anisotropy.

2.4. Conclusions

In summary, we have demonstrated a large room temperature spin lifetime anisotropy of $\xi \geqslant 60$ in BLG spin valves proximity-coupled to WSe_2. Through a combination of Hanle and oblique spin precession measurements and supported by numerical simulations, we determined that the out-of-plane spin lifetime in the BLG/WSe_2 region is approximately 250–300 ps, whereas the in-plane spin lifetime is suppressed below 4 ps. The latter effectively eliminates transport of in-plane spins, allowing only the out-of-plane oriented spins to propagate in the direction of the spin detector. The achieved spin lifetime anisotropy of 60 is the highest at 300 K reported so far for graphene-based heterostructures. At the same time, the determined anisotropy factor represents a conservative lower bound of what can be achieved in a BLG/WSe_2 heterostructure, as substrate- and contact-induced spin relaxation processes have likely limited the measured out-of-plane spin lifetime. We attribute the large spin lifetime anisotropy to the use of BLG, which is predicted to exhibit significantly higher anisotropy compared to SLG [4, 25].

Data availability statement

The data that support the findings of this study are openly available at https://doi.org/10.5281/zenodo.15609970 [63].

Simulations of Hanle effect available at https://doi.org/10.1088/2053-1583/ae2d6b/data1.

Acknowledgments

This project has received funding from the European Union's Horizon 2020 research and innovation programme under Grant Agreement No. 881603 (Graphene Flagship), the Deutsche Forschungsgemeinschaft (DFG, German Research Foundation) under Germany's Excellence Strategy—Cluster of Excellence Matter and Light for Quantum Computing (ML4Q) EXC 2004/1—390534769 and by the Helmholtz Nano Facility [64] at the Forschungszentrum Jülich.

ORCID iDs

Frank Volmer 0000-0003-3526-2687
Christoph Stampfer 0000-0002-4958-7362
Bernd Beschoten 0000-0003-2359-2718

References

[1] Gmitra M and Fabian J 2015 Graphene on transition-metal dichalcogenides: a platform for proximity spin-orbit physics and optospintronics *Phys. Rev. B* **92** 155403
[2] Roche S *et al* 2015 Graphene spintronics: the European Flagship perspective *2D Mater.* **2** 030202
[3] Zollner K, Kurpas M, Gmitra M and Fabian J 2025 First-principles determination of spin-orbit coupling parameters in two-dimensional materials *Nat. Rev. Phys.* **7** 255
[4] Gmitra M and Fabian J 2017 Proximity effects in bilayer graphene on monolayer WSe_2: field-effect spin valley locking, spin-orbit valve and spin transistor *Phys. Rev. Lett.* **119** 146401
[5] Wang Z, Ki D-K, Khoo J Y, Mauro D, Berger H, Levitov L S and Morpurgo A F 2016 Origin and magnitude of designer spin-orbit interaction in graphene on semiconducting transition metal dichalcogenides *Phys. Rev. X* **6** 041020
[6] Khatibi Z and Power S R 2022 Proximity spin-orbit coupling in graphene on alloyed transition metal dichalcogenides *Phys. Rev. B* **106** 125417

[7] Zollner K and Fabian J 2024 Proximity effects, topological states and correlated physics in graphene heterostructures *2D Mater.* **12** 013004

[8] Karpiak B *et al* 2019 Magnetic proximity in a van der Waals heterostructure of magnetic insulator and graphene *2D Mater.* **7** 015026

[9] Naimer T and Fabian J 2023 Twist-angle dependent proximity induced spin-orbit coupling in graphene/topological insulator heterostructures *Phys. Rev. B* **107** 195144

[10] Cummings A W, Garcia J H, Fabian J and Roche S 2017 Giant spin lifetime anisotropy in graphene induced by proximity effects *Phys. Rev. Lett.* **119** 206601

[11] Offidani M and Ferreira A 2018 Microscopic theory of spin relaxation anisotropy in graphene with proximity-induced spin-orbit coupling *Phys. Rev. B* **98** 245408

[12] Benítez L A, Sierra J F, Savero Torres W, Timmermans M, Costache M V and Valenzuela S O 2019 Investigating the spin-orbit interaction in van der Waals heterostructures by means of the spin relaxation anisotropy *APL Mater.* **7** 120701

[13] Benítez L A, Sierra J F, Savero Torres W, Arrighi A, Bonell F, Costache M V and Valenzuela S O 2018 Strongly anisotropic spin relaxation in graphene-transition metal dichalcogenide heterostructures at room temperature *Nat. Phys.* **14** 303

[14] Ghiasi T S, Ingla-Aynés J, Kaverzin A A and van Wees B J 2017 Large proximity-induced spin lifetime anisotropy in transition-metal dichalcogenide/graphene heterostructures *Nano Lett.* **17** 7528–32

[15] Hoque A M *et al* 2023 Spin-valley coupling and spin-relaxation anisotropy in all-CVD graphene-MoS_2 van der Waals heterostructure *Phys. Rev. Mater.* **7** 044005

[16] Sierra J F *et al* 2025 Room-temperature anisotropic in-plane spin dynamics in graphene induced by $PdSe_2$ proximity *Nat. Mater.* **24** 876

[17] Ingla-Aynés J, Herling F, Fabian J, Hueso L E and Casanova F 2021 Electrical control of Valley-Zeeman spin-orbit-coupling-induced spin precession at room temperature *Phys. Rev. Lett.* **127** 047202

[18] Herling F, Safeer C K, Ingla-Aynés J, Ontoso N, Hueso L E and Casanova F 2020 Gate tunability of highly efficient spin-to-charge conversion by spin Hall effect in graphene proximitized with WSe_2 *APL Mater.* **8** 071103

[19] Zihlmann S, Cummings A W, Garcia J H, Kedves M, Watanabe K, Taniguchi T, Schönenberger C and Makk P 2018 Large spin relaxation anisotropy and Valley-Zeeman spin-orbit coupling in WSe_2/graphene/h-BN heterostructures *Phys. Rev. B* **97** 075434

[20] Island J O *et al* 2019 Spin-orbit-driven band inversion in bilayer graphene by the van der Waals proximity effect *Nature* **571** 85

[21] Seiler A M *et al* 2025 Layer-selective spin-orbit coupling and strong correlation in bilayer graphene *2D Mater.* **12** 035009

[22] Icking E, Wörtche F, Cummings A W, Wörtche A, Watanabe K, Taniguchi T, Volk C, Beschoten B and Stampfer C 2025 Weak localization as probe of spin-orbit-induced spin-split bands in bilayer graphene proximity coupled to WSe_2 (arXiv:2505.24632)

[23] Icking E *et al* 2022 Transport spectroscopy of ultraclean tunable band gaps in bilayer graphene *Adv. Electron. Mater.* **8** 2200510

[24] Khoo J Y, Morpurgo A F and Levitov L 2017 On-demand spin-orbit interaction from which-layer tunability in bilayer graphene *Nano Lett.* **17** 7003

[25] Omar S, Madhushankar B N and van Wees B J 2019 Large spin-relaxation anisotropy in bilayer-graphene/WS_2 heterostructures *Phys. Rev. B* **100** 155415

[26] Banszerus L, Janssen H, Otto M, Epping A, Taniguchi T, Watanabe K, Beschoten B, Neumaier D and Stampfer C 2017 Identifying suitable substrates for high-quality graphene-based heterostructures *2D Mater.* **4** 025030

[27] Banszerus L *et al* 2019 Extraordinary high room-temperature carrier mobility in graphene-WSe_2 heterostructures (arXiv:1909.09523)

[28] Raes B, Scheerder J E, Costache M V, Bonell F, Sierra J F, Cuppens J, Van de Vondel J and Valenzuela S O 2016 Determination of the spin-lifetime anisotropy in graphene using oblique spin precession *Nat. Commun.* **7** 11444

[29] Raes B, Cummings A W, Bonell F, Costache M V, Sierra J F, Roche S and Valenzuela S O 2017 Spin precession in anisotropic media *Phys. Rev. B* **95** 085403

[30] Zhu T, Singh S, Katoch J, Wen H, Belashchenko K, Žutić I and Kawakami R K 2018 Probing tunneling spin injection into graphene via bias dependence *Phys. Rev. B* **98** 054412

[31] Xu J, Zhu T, Luo Y K, Lu Y-M and Kawakami R K 2018 Strong and tunable spin-lifetime anisotropy in dual-gated bilayer graphene *Phys. Rev. Lett.* **121** 127703

[32] Bisswanger T, Winter Z, Schmidt A, Volmer F, Watanabe K, Taniguchi T, Stampfer C and Beschoten B 2022 CVD bilayer graphene spin valves with 26 μm spin diffusion length at room temperature *Nano Lett.* **22** 4949–55

[33] Volmer F, Drögeler M, Maynicke E, von den Driesch N, Boschen M L, Güntherodt G and Beschoten B 2013 Role of MgO barriers for spin and charge transport in Co/MgO/graphene nonlocal spin-valve devices *Phys. Rev. B* **88** 161405

[34] Volmer F, Drögeler M, Maynicke E, von den Driesch N, Boschen M L, Güntherodt G, Stampfer C and Beschoten B 2014 Suppression of contact-induced spin dephasing in graphene/MgO/Co spin-valve devices by successive oxygen treatments *Phys. Rev. B* **90** 165403

[35] Volmer F, Seidler I, Bisswanger T, Tu J-S, Schreiber L R, Stampfer C and Beschoten B 2021 How to solve problems in micro- and nanofabrication caused by the emission of electrons and charged metal atoms during e-beam evaporation *J. Appl. Phys.* **54** 225304

[36] Leven B and Dumpich G 2005 Resistance behavior and magnetization reversal analysis of individual Co nanowires *Phys. Rev. B* **71** 064411

[37] Brands M and Dumpich G 2005 Experimental determination of anisotropy and demagnetizing factors of single Co nanowires by magnetoresistance measurements *J. Appl. Phys.* **98** 014309

[38] Stoner E C and Wohlfarth E P 1948 A mechanism of magnetic hysteresis in heterogeneous alloys *Phil. Trans. R. Soc. A* **240** 599

[39] Leutenantsmeyer J C, Ingla-Aynés J, Fabian J and van Wees B J 2018 Observation of spin-valley-coupling-induced large spin-lifetime anisotropy in bilayer graphene *Phys. Rev. Lett.* **121** 127702

[40] Volmer F, Bisswanger T, Schmidt A, Stampfer C and Beschoten B 2022 Charge-induced artifacts in nonlocal spin-transport measurements: how to prevent spurious voltage signals *Phys. Rev. Appl.* **18** 014028

[41] Ouaj T *et al* 2024 Benchmarking the integration of hexagonal boron nitride crystals and thin films into graphene-based van der Waals heterostructures *2D Mater.* **12** 015017

[42] Johnson M and Silsbee R H 1988 Coupling of electronic charge and spin at a ferromagnetic-paramagnetic metal interface *Phys. Rev. B* **37** 5312

[43] Fabian J, Matos-Abiague A, Ertler C, Stano P and Žutić I 2007 Semiconductor spintronics *Acta Phys. Slov.* **57** 565

[44] Volmer F, Drögeler M, Pohlmann T, Güntherodt G, Stampfer C and Beschoten B 2015 Contact-induced charge contributions to non-local spin transport measurements in Co/MgO/graphene devices *2D Mater.* **2** 024001

[45] Ringer S, Hartl S, Rosenauer M, Völkl T, Kadur M, Hopperdietzel F, Weiss D and Eroms J 2018 Measuring anisotropic spin relaxation in graphene *Phys. Rev. B* **97** 205439

[46] Zhu T and Kawakami R K 2018 Modeling the oblique spin precession in lateral spin valves for accurate determination of the spin lifetime anisotropy: effect of finite contact resistance and channel length *Phys. Rev. B* **97** 144413

[47] Maassen T, Vera-Marun I J, Guimarães M H D and van Wees B J 2012 Contact-induced spin relaxation in Hanle spin precession measurements *Phys. Rev. B* **86** 235408
[48] Stecklein G, Crowell P A, Li J, Anugrah Y, Su Q and Koester S J 2016 Contact-induced spin relaxation in graphene nonlocal spin valves *Phys. Rev. Appl.* **6** 054015
[49] Drögeler M, Volmer F, Stampfer C and Beschoten B 2017 Simulations on the influence of spatially varying spin transport parameters on the measured spin lifetime in graphene non-local spin valves *Phys. Status Solidi b* **254** 1700293
[50] Sosenko E, Wei H and Aji V 2014 Effect of contacts on spin lifetime measurements in graphene *Phys. Rev. B* **89** 245436
[51] Amamou W, Lin Z, van Baren J, Turkyilmaz S, Shi J and Kawakami R K 2016 Contact induced spin relaxation in graphene spin valves with $Al2O_3$ and MgO tunnel barriers *APL Mater.* **4** 032503
[52] Habib A, Xu J, Ping Y and Sundararaman R 2022 Electric fields and substrates dramatically accelerate spin relaxation in graphene *Phys. Rev. B* **105** 115122
[53] Van Tuan D, Ortmann F, Cummings A W, Soriano D and Roche S 2016 Spin dynamics and relaxation in graphene dictated by electron-hole puddles *Sci. Rep.* **6** 21046
[54] Ertler C, Konschuh S, Gmitra M and Fabian J 2009 Electron spin relaxation in graphene: the role of the substrate *Phys. Rev. B* **80** 041405
[55] Drögeler M, Franzen C, Volmer F, Pohlmann T, Banszerus L, Wolter M, Watanabe K, Taniguchi T, Stampfer C and Beschoten B 2016 Spin lifetimes exceeding 12 ns in graphene nonlocal spin valve devices *Nano Lett.* **16** 3533
[56] Li Y and Koshino M 2019 Twist-angle dependence of the proximity spin-orbit coupling in graphene on transition-metal dichalcogenides *Phys. Rev. B* **99** 075438
[57] Pezo A, Zanolli Z, Wittemeier N, Ordejón P, Fazzio A, Roche S and Garcia J H 2021 Manipulation of spin transport in graphene/transition metal dichalcogenide heterobilayers upon twisting *2D Mater.* **9** 015008
[58] Péterfalvi C G, David A, Rakyta P, Burkard G and Kormányos A 2022 Quantum interference tuning of spin-orbit coupling in twisted van der Waals trilayers *Phys. Rev. Res.* **4** L022049
[59] Lee S, de Sousa D J P, Kwon Y-K, de Juan F, Chi Z, Casanova F and Low T 2022 Charge-to-spin conversion in twisted graphene/WSe_2 heterostructures *Phys. Rev. B* **106** 165420
[60] Zollner K, João S M, Nikolić B K and Fabian J 2023 Twist- and gate-tunable proximity spin-orbit coupling, spin relaxation anisotropy and charge-to-spin conversion in heterostructures of graphene and transition metal dichalcogenides *Phys. Rev. B* **108** 235166
[61] Yang H, Martín-García B, Kimák J, Schmoranzerová E, Dolan E, Chi Z, Gobbi M, Němec P, Hueso L E and Casanova F 2024 Twist-angle-tunable spin texture in WSe_2/graphene van der Waals heterostructures *Nat. Mater.* **23** 1502
[62] Frank T, Faria Junior P E, Zollner K and Fabian J 2024 Emergence of radial Rashba spin-orbit fields in twisted van der Waals heterostructures *Phys. Rev. B* **109** L241403
[63] Bisswanger T, Schmidt A, Volmer F, Stampfer C and Beschoten B 2025 Data repository for the manuscript: room-temperature spin-lifetime anisotropy exceeding 60 in bilayer graphene spin valves proximity coupled to WSe_2 [Data set] *Zenodo* (https://doi.org/10.5281/zenodo.15609970)
[64] Albrecht W, Moers J and Hermanns B 2017 HNF-helmholtz nano facility *J. Large-Scale Res. Facil. JLSRF* **3** 112